

EAS-SNN: End-to-End Adaptive Sampling and Representation for Event-based Detection with Recurrent Spiking Neural Networks

Ziming Wang¹, Ziling Wang¹, Huaning Li¹, Lang Qin¹, Runhao Jiang¹,
De Ma^{1,2}, and Huajin Tang^{1,2}

¹ College of Computer Science, Zhejiang University, Hangzhou 310027, China

² State Key Laboratory of Brain-Machine Intelligence, Zhejiang University,
Hangzhou 310027, China

{zi_ming_wang, wzzero.hhh, lhnkevin1014, qinl, RhJiang, made, htang}@zju.edu.cn

Abstract. Event cameras, with their high dynamic range and temporal resolution, are ideally suited for object detection, especially under scenarios with motion blur and challenging lighting conditions. However, while most existing approaches prioritize optimizing spatiotemporal representations with advanced detection backbones and early aggregation functions, the crucial issue of adaptive event sampling remains largely unaddressed. Spiking Neural Networks (SNNs), which operate on an event-driven paradigm through sparse spike communication, emerge as a natural fit for addressing this challenge. In this study, we discover that the neural dynamics of spiking neurons align closely with the behavior of an ideal temporal event sampler. Motivated by this insight, we propose a novel adaptive sampling module that leverages recurrent convolutional SNNs enhanced with temporal memory, facilitating a fully end-to-end learnable framework for event-based detection. Additionally, we introduce Residual Potential Dropout (RPD) and Spike-Aware Training (SAT) to regulate potential distribution and address performance degradation encountered in spike-based sampling modules. Through rigorous testing on neuromorphic datasets for event-based detection, our approach demonstrably surpasses existing state-of-the-art spike-based methods, achieving superior performance with significantly fewer parameters and time steps. For instance, our method achieves a 4.4% mAP improvement on the Gen1 dataset, while requiring 38% fewer parameters and three time steps. Moreover, the applicability and effectiveness of our adaptive sampling methodology extend beyond SNNs, as demonstrated through further validation on conventional non-spiking detection models.

Keywords: Event-based Vision · Spiking Neural Network · Neuromorphic Computing

1 Introduction

Event cameras, inspired by biological vision systems, present a transformative approach to dynamic visual sensing. Diverging from the conventional imaging

model, where cameras capture scene illumination synchronously via a global shutter, event cameras operate on an asynchronous basis, logging logarithmic intensity changes at the pixel level. Each significant change in this context is referred to as an "event". This distinct operational paradigm grants event cameras extraordinary capabilities: exceptional temporal resolution ($>10\text{k}$ fps), high dynamic range (>120 dB), and remarkably low power consumption (<10 mW) [15, 16, 37, 50]. These attributes render event cameras exceptionally suited for object detection under challenging environments characterized by rapid motion, extreme lighting conditions, or stringent energy constraints.

However, the inherent asynchronous and sparse characteristics of data captured by event cameras present significant obstacles for traditional dense neural networks, which are primarily designed to process synchronous, uniformly structured data. To reconcile the asynchronous event stream with the dense tensor formats utilized in ANNs, most existing frameworks incorporate a sampling-aggregation mechanism, also referred to as event representation or embedding [3, 18, 19, 30, 38]. This integration effectively alleviates the computational demands engendered by the high temporal resolution of event data. Building upon this foundation, researchers have delved into exploiting the unique spatiotemporal attributes of event data through refining event representations [8, 31, 32, 34, 52] and enhancing the design of detection architectures [19, 22, 32, 41, 46, 49, 53], thereby boosting network efficacy. Additionally, the aggregation module is integrated with downstream feature extraction components into a unified end-to-end training framework [18]. Regarding event-based sampling, several studies have endeavored to enhance the sampling module from a rule-based or search-based perspective [5, 32, 38, 69]. Nonetheless, these initiatives frequently suffer from the lack of high-level semantic information or are encumbered by artificial constraints and suboptimal search efficiency. So far, the quest for a differentiable, adaptive sampling module that facilitates end-to-end optimization within event-based detection frameworks remains unfulfilled.

On the other hand, SNNs, composed of biologically plausible spiking neurons, support asynchronous event-driven computation on neuromorphic architectures [1, 9, 45] and so present a high potential for fast inference and low power consumption. This positions SNNs as inherently compatible with the sparse nature of event data. Moreover, a spectrum of low-level representations [18, 31, 52] potentially allows for their encapsulation within a unified SNN layer [28]. Nevertheless, the challenge of training deep SNNs under long time steps persists, in spite of rapid advancements in spike-based learning algorithm [14, 35, 39, 51, 55, 58, 62, 68]. This makes it difficult to align the discretization window of SNNs with event response time, culminating in a discernible information temporal information loss. Therefore, the current event-based detection models based on SNNs exhibit a notable performance discrepancy when compared to their ANN counterparts.

To address these challenges, this work introduces ARSNN, a learnable adaptive sampling methodology with recurrent convolutional SNNs (Fig. 1a), enabling a comprehensive end-to-end learning paradigm for event representation and feature extraction. This methodology utilizes pixel-wise spiking neurons in

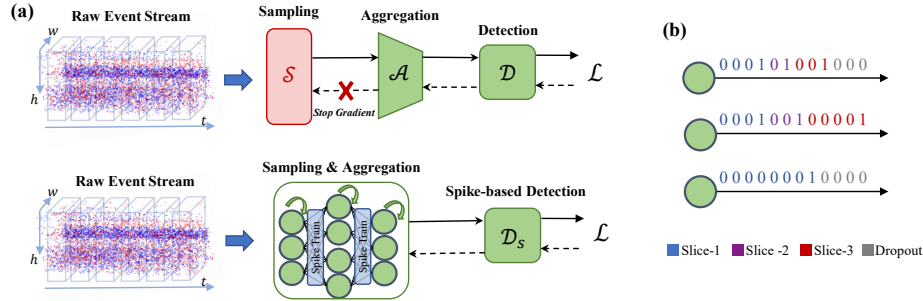


Fig. 1: *Left:* Implementing the end-to-end optimization for event-based sampling via introducing recurrent SNNs. It highlights how typical rule-based methods truncate back-propagation, inhibiting optimization, whereas our adaptive sampling module ensures continuous gradient flow. *Right:* The variability in sampling time and count among different spiking neurons, emphasizes the heterogeneity inherent in our approach.

the sampling module to capture the dynamic information delivered by events across receptive fields. Upon the information integration surpassing a predefined threshold, the events between the last and the current spike firing times are sampled as shown in Fig. 1b. By optimizing the spike firing time and membrane potential distribution, the sampling module can be trained and coordinated with downstream spike-based detectors, thereby greatly mitigating the temporal alignment loss between the raw event stream and SNNs. Moreover, the proposed SNN-based approach is optimally positioned for deployment on neuromorphic hardware, potentially curtailing overhead from data migration. The main contributions are outlined as follows:

1. We first propose a learnable adaptive sampling method and realize an end-to-end event-based detection framework via SNNs that seamlessly integrates the processes of sampling, aggregation, and feature extraction.
2. We develop the techniques of Residual Potential Dropout (RPD) and Spike-Aware Training (SAT) to mitigate the performance degradation problem in SNN-based sampling modules with the recurrent convolutional architecture.
3. Empirical evaluations on neuromorphic datasets (N-Caltech 101 and Gen1) show the proposed method achieves superior performance over the state-of-the-art spike-based methods with $5.85\times$ less energy consumption compared to ANNs. Furthermore, the effectiveness of our adaptive sampling method is verified across dense detection models.

2 Related Work

2.1 Spiking Neural Networks

Spiking Neural Networks (SNNs) have raised substantial interest due to their asynchronous computation paradigm and promising energy efficiency. However,

optimizing SNNs poses challenges, particularly due to the binary nature of spike firing. The advancements in backpropagation techniques for SNNs, including time-based [42, 43, 63, 64, 67] and activation-based methods [7, 20, 35, 51, 55, 58, 62], estimate gradients for firing time and spike generation successfully. Additionally, various spiking neuron models [6, 14, 21, 24, 36, 60] have been proposed to enhance network heterogeneity and performance. To maintain gradient flow in deep SNNs, specialized network modules [11, 14, 65] and architectures [13, 27, 53, 59, 66] have been developed considering temporal dynamics in spiking neurons. These collective efforts are narrowing the performance gap between SNNs and ANNs in various tasks, including object detection [53, 61], point cloud recognition [48], and automatic speech recognition [57].

2.2 Event-based Detection

In event-based detection, methodologies are bifurcated into two principal categories: dense and sparse representations. Dense representations typically convert event data into frame-based formats, subsequently processed by conventional dense detection algorithms [3, 4, 19, 30, 38]. This approach, while facilitating the utilization of pre-trained models within an event-based context [40], tends to significantly compress the inherent spatiotemporal richness of events, necessitating sophisticated event-to-frame conversion techniques. In pursuit of more effectively extracting the spatiotemporal information from event streams, researchers have integrated the recurrent connections [19, 32, 46] and attention mechanisms [33, 54]. Recent advancements [19, 22, 38] strive to minimize detection latency without substantial performance degradation, through the strategic redesign of network backbones and event aggregation modules, thus enhancing adaptability to scenarios demanding high-speed processing.

Conversely, sparse representations, embodied by Graph Neural Networks (GNNs) and SNNs, offer substantial energy efficiency due to their inherent sparse computational models. GNN models [34, 49] construct dynamic spatio-temporal graphs from event stream, updating node and edge states with incoming events. In parallel, SNN methodologies [8, 53, 61], characterized by the internal temporal dynamics and spike-driven computation, naturally complement the asynchronous nature of event stream. However, given the high temporal resolution of event cameras, event-based sampling is imperative to mitigate computational demands and enhance network generalization capabilities, even for sparse representation.

For event-based sampling, a spectrum of methodologies has emerged to refine rule-based strategies, taking into account the instantaneous rate of event generation [29, 32, 38]. Nevertheless, these strategies routinely encounter challenges associated with hyperparameter sensitivity, as well as the difficulty of maintaining an optimal balance between sparse and ambiguous textures in complex scenarios. Nikola *et al.* [69] have explored the optimization of sampling windows based on the Gromov-Wasserstein discrepancy from raw event data to their representations. Nonetheless, the technique has yet not fully integrated high-level semantic guidance. Cao *et al.* [5] have proposed the use of SNNs as a mechanism

for global event triggering, advocating for a feedback-update mechanism that employs pseudo labels generated by downstream detectors to guide SNN training. Despite these advancements, the integration of ANNs and SNNs remains disjointed, bridged solely by pseudo labels, which introduces artificial constraints on the optimization landscape and compromises search efficiency. In this work, we investigate an adaptive event sampling strategy leveraging learnable SNNs, marking a step towards achieving comprehensive end-to-end event-based representation learning.

3 Methodology

3.1 Event-based Detection

Consider an event stream denoted as $\mathbf{E} = \{(x_i, y_i, p_i, t_i)\}_{i \in \mathbb{N}}$, where each event e_i is characterized by its spatial coordinates $x_i \in [1, W]$ and $y_i \in [1, H]$, a polarity value $p_i \in \{-1, 1\}$ indicating the change in pixel intensity, and a timestamp $t_i \in [0, +\infty)$ marking the occurrence time of events (typically measured in microseconds). In event-based detection, annotations at a specific target time t include object categories l_j and associated ground truth bounding boxes (x_j, y_j, w_j, h_j) , encapsulated as $\mathbf{B}_t = (x_j, y_j, w_j, h_j, l_j, t)_{j \in \mathbb{N}}$. Ideally, a real-time detector \mathcal{D} is capable of delivering predictions at the timestamp level:

$$\mathcal{D}(\mathbf{E}) = \{\mathcal{D}(\mathbf{E}, t)\}_{t \geq 0} = \{\mathcal{D}(\{e_i\}_{t_i < t})\}_{t \geq 0} \quad (1)$$

Nonetheless, given the high temporal resolution of event cameras, it is challenging for event-based object detectors to process and interpret $10^4 - 10^5$ times per second. Moreover, the necessity for detecting moving objects at microsecond intervals is often not critical, as object motion typically occurs at a slower pace than the pixel response rate of event cameras [46]. Consequently, the current body of literature [19, 32, 53, 61] frequently incorporates a sampling operation \mathcal{S} and an aggregation operation \mathcal{A} to reduce the volume of sparse and asynchronous event data, thereby facilitating more efficient processing prior to the detection phase:

$$\hat{\mathcal{D}}(\mathbf{E}, t) = (\mathcal{D} \circ \mathcal{A} \circ \mathcal{S})(\mathbf{E}, t) = (\mathcal{D} \circ \mathcal{A} \circ \mathcal{S})(\{e_i\}_{t_i < t}) \quad (2)$$

By employing fixed window sampling as an example, \mathcal{S} can be expressed as:

$$\mathcal{S}_{\Delta t, T}(\{e_i\}_{t_i < t}) = \Omega_{\Delta t, T} = \{\{e_i\}_{t - (j+1)\Delta t \leq t_i \leq t - j\Delta t}\}_{j \in [0, T/\Delta t]} \quad (3)$$

In this formula, T denotes the global time window for sampling, and Δt represents the interval of sampling slices. We designate the collection of events that meet the criteria for fixed window sampling within the j -th step as \mathbf{S}_j . For the j -th step sampling, a typical aggregation function, \mathcal{A}^j , based on event count histograms, is defined as follows:

$$\mathcal{A}^j(\{e_i\}_{i \in \mathbf{S}_j}) = f_j(x, y, p) = \sum_{i \in \mathbf{S}_j} \delta(x - x_i, y - y_i, p - p_i) \quad (4)$$

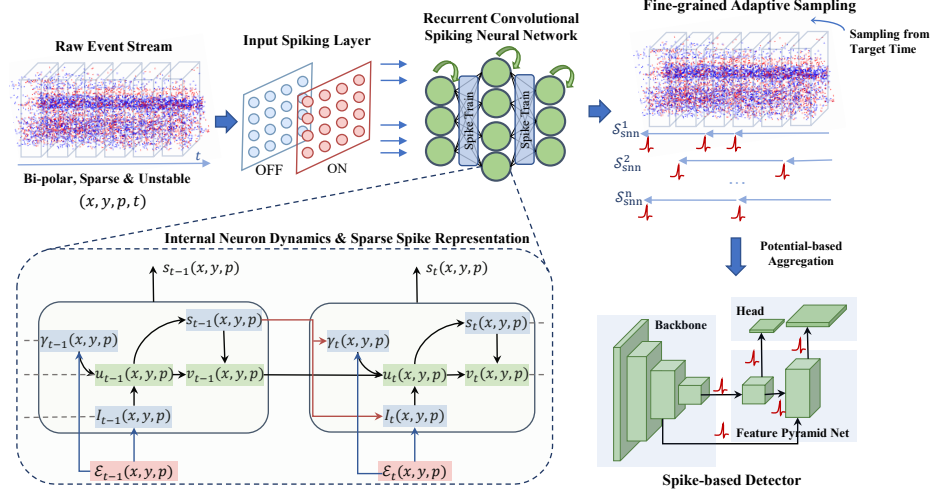


Fig. 2: Illustration of the overall pipeline. The adaptive sampling module, augmented with recurrent synaptic connections for improved memory mechanism, seamlessly interfaces the input event stream with the downstream spike-based detection network. Within the unrolled graph of a spiking neuron, internal neuron dynamics are indicated by solid black lines, while blue and red solid lines depict the feedforward and recurrent pathways, respectively.

Here, $\delta(x, y, z)$ represents the Dirac delta function, which equals 1 only when $x = y = z = 0$. By employing this approach, the asynchronous and sparse event data are effectively down-sampled into a compact form that significantly alleviates the computational burden on the detector. However, existing sampling techniques often operate independently of downstream object detectors or multi-scale feature extractors, necessitating extensive hyperparameter tuning and showing limited adaptability.

3.2 Recurrent Convolutional SNNs for Adaptive Event Sampling

In this study, our goal is to develop a learnable sampling module, denoted as \mathcal{S}_{SNN} , utilizing SNNs to address the challenge of non-differentiable, end-to-end learning that constrains rule-based sampling methods.

The leaky-integrate-and-fire (LIF) model, popular in neuromorphic computing due to its minimal computational requirements, serves as the foundation for our approach. This model is mathematically expressed as follows:

$$\tau_m \frac{du_i^\ell(t)}{dt} = -u_i^\ell(t) + RI_i^\ell(t) \quad (5)$$

Here, $u_i^\ell(t)$ and $I_i^\ell(t)$ denote the membrane potential and input current of the i -th neuron in the l -th layer, respectively, with τ_m representing the membrane time constant. Upon receiving spike inputs, a neuron accumulates the input

current $I_i^\ell(t)$ into its membrane potential $u_i^\ell(t)$ which decays at a constant rate. A spike is emitted, and the membrane potential is reset when $u_i^\ell(t)$ exceeds the threshold θ . We denote the membrane potential after reset as $v_i^\ell(t)$. The discrete representation of the LIF model via the first-order Euler method, with a time slice of Δt_s , is given by:

$$u_i^\ell[t] = g(v_i^\ell[t-1], I_i^\ell[t]) = (1 - \frac{\Delta t_s}{\tau_m})v_i^\ell[t-1] + \frac{\Delta t_s}{\tau_m}I_i^\ell[t] \quad (6)$$

$$s_i^l[t] = \Theta(u_i^\ell[t] - \theta) = \begin{cases} 1, & u_i^\ell[t] \geq \theta, \\ 0, & u_i^\ell[t] < \theta \end{cases} \quad (7)$$

$$v_i^\ell[t] = \begin{cases} u_i^\ell[t] - \theta \cdot s_i^l[t], & \text{soft reset} \\ u_i^\ell[t] \cdot (1 - s_i^l[t]) + u_{\text{reset}} \cdot s_i^l[t], & \text{hard reset} \end{cases} \quad (8)$$

This leaky-integrate-and-fire dynamic closely aligns with the desired properties of an event sampler. A subset of events should be selectively sampled as the accumulated information from the asynchronous event stream reaches a certain threshold. Consequently, we associate the spike firing in SNNs with event-based sampling, integrating this functionality into an end-to-end optimization framework as shown in Fig. 2.

Firstly, restricted by the poor support for sparse spike-driven computation on GPUs, we perform early aggregation using event count as shown in Eq. (4) with a small time slice Δt_m and obtain the actual T_m -step inputs for \mathcal{S}_{SNN} . It is worth noting that in general, the closer the timestamps of events are to the detection target timestamp t' , the greater the impact on the detection result at t' . Therefore, in this case, the input closer to t' in time is preferentially sent to \mathcal{S}_{SNN} . This operation is also consistent with the temporal information dynamics in the SNNs which has been observed that information becomes highly concentrated in earlier few timesteps [26]. Following early aggregation, a distinct spiking neuron is allocated to each spatial position (x, y) and polarity p , with each neuron exhibiting unique behavior by accumulating its spatially localized input over time.

$$\begin{aligned} I_t(x, y, p) &= (W_{\text{conv}} * f_t)(x, y, p) + b_{\text{conv}}(p) \\ u_t(x, y, p) &= g(I_t(x, y, p), v_t(x, y, p)) = \gamma \cdot v_t(x, y, p) + I_t(x, y, p) \end{aligned} \quad (9)$$

where $\gamma = 1 - \frac{\Delta t_s}{\tau_m}$ denotes a constant decay factor. Our empirical findings suggest that an effective sampler must possess an advanced temporal credit assignment capability to extract informative and discriminative substreams from the inherently noisy and fluctuating spatiotemporal event data. Consequently, we incorporate recurrent synapse connections, as depicted in the bottom left portion of Fig. 2, to enhance the temporal representational capacity of SNNs:

$$\begin{aligned} u_t(x, y, p) &= g(I_t(x, y, p), v_{t-1}(x, y, p)) = \gamma_t(x, y, p) \cdot v_{t-1}(x, y, p) + I_t(x, y, p) \\ I_t(x, y, p) &= (W_I^f * f_t)(x, y, p) + (W_I^s * s_{t-1})(x, y, p) + b_I(p) \\ \gamma_t(x, y, p) &= \sigma((W_\gamma^f * f_t)(x, y, p) + (W_\gamma^s * s_{t-1})(x, y, p) + b_\gamma(p)) \end{aligned} \quad (10)$$

Here, the spike firing $s_{t-1}(x, y, p)$ at the last time step contributes to the input current $I_t(x, y, p)$ and decay factor $\gamma_t(x, y, p)$ at the current time step directly through recurrent synapse W_I^s and W_γ^s . σ denotes the sigmoid function which normalizes the decay factor γ_t . We refer to SNNs after this modification as ‘‘RSNN’’ compared to Eq. (9), which effectively helps improve detection performance. When the spike is emitted with over-threshold membrane potential, the event slice between the last spike firing time $t^{k-1}(x, y, p)$ and the current spike firing time $t^k(x, y, p)$ is sampled, so as to achieve local sampling:

$$\Omega^k(x, y, p) = \{(x_i, y_i, p_i, t_i) | t_i \in (t^{k-1}(x, y, p), t^k(x, y, p)) \ \& \ [x, y, p] = [x_i, y_i, p_i]\} \\ \text{where } s_{t^k}(x, y, p) = 1 \ \& \ t^{k-1}(x, y, p) < t^k(x, y, p) \quad (11)$$

This approach infuses the adaptability into event sampling, driven by the inherent variability in firing times across spiking neurons located at distinct spatial coordinates. Notably, we adopt the hard reset to clear the membrane potential from the last sample. Following the event-based sampling phase, the subsequent challenge is to effectively integrate each sampled set into a coherent embedding. Empirically, we find that decoupling the sampling and the aggregation modules might hinder the training phase due to unstable gradient flow. Hence, in this work, we unify the sampling and the aggregation within a singular SNN. We directly employ the accumulation of membrane potential within the specified sampling window $(t^{k-1}[x, y, p], t^k[x, y, p])$ as the aggregation input for the downstream network:

$$\hat{f}_k(x, y, p) = \sum_{(x_i, y_i, p_i, t_i) \in \Omega^k(x, y, p)} u_{t_i}(x_i, y_i, p_i) \quad (12)$$

Such a model incorporating the spike-driven sampling mechanism and the synaptic recurrent connection is referred to as the ‘ARSNN’ for the latter discussion.

3.3 Mitigating Degradation of Spike-based Sampling

In light of the adaptive sampling, it can be seamlessly integrated with the downstream detector for end-to-end training via backpropagation through time (BPTT) [56] with surrogate gradient functions [14, 51, 58]. Nonetheless, this aggregation of Eq. (12) implicitly optimizes the sampling module by relying solely on the aggregation of membrane potentials, which lacks information from the firing threshold for optimizing the spike firing timing. To elucidate, we leverage the gradients from the activation-based technique in SNN training to compute the update of firing time t^k (detailed derivation provided in the Supplementary Material):

$$\Delta t^k(x, y, p) \propto - \frac{\partial \mathcal{L}((\mathcal{D} \circ \mathcal{A} \circ \mathcal{S})(\mathbf{E}, t), \mathbf{B}_t)}{\partial \hat{f}_k(x, y, p)} (u_{t^k}(x, y, p) - u_{t^{k-1}}(x, y, p)) \quad (13)$$

This reveals that the adjustment in firing time t^k is solely dependent on the gradient of the membrane potential $u_{t^k}(x, y, p)$ and the instantaneous change

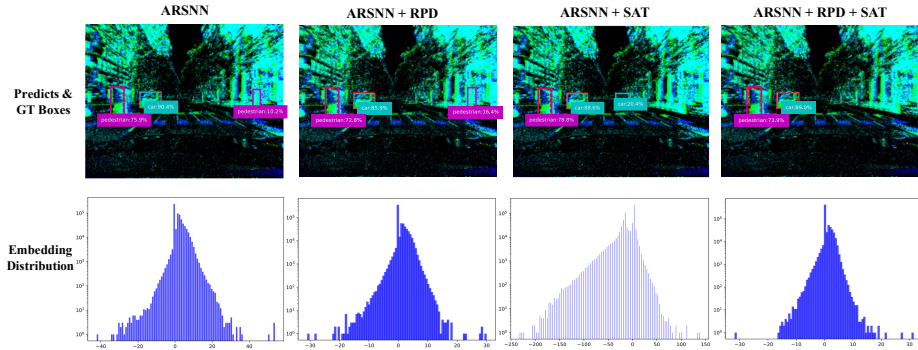


Fig. 3: Visualizing the detection results and corresponding embedding distributions of different models in ablation study. The red dashed line highlights the ground truth.

in potential at the firing moment. It disregards the relationship between the firing time update Δt^k with the firing threshold θ . To counteract this issue, we introduce Spike-aware Training (SAT), which incorporates the firing spike $s_{t^k}(x, y, p)$ into the aggregation function:

$$\hat{f}_k(x, y, p) = s_{t^k}(x, y, p) \sum_{t'=t^{k-1}(x, y, p)+1}^{t^k(x, y, p)} u_{t'}(x, y, p) \quad (14)$$

Given $s_{t^k} = 1$, this modification does not alter the forward computation of the aggregation function. However, it effectively rewires the gradient flow:

$$\Delta t^k \propto -\frac{\partial \mathcal{L}}{\partial \hat{f}_k} (1 + u_{t^k} h_\alpha(u_{t^k} - \theta))(u_{t^k} - u_{t^k-1}), \quad \forall (x, y, p) \quad (15)$$

where $h_\alpha(x)$ is the surrogate gradient function used for circumventing the non-differential problem of the Heaviside function of Eq. (7). Here, $1 + u_{t^k} h_\alpha(u_{t^k} - \theta)$ represents the adjustment from threshold-based gradient redirection, enhancing the update of firing time $s_{t^k}(x, y, p)$ especially when near the threshold θ , thereby achieving a more precise sampling away from critical points.

Moreover, the implementation of a spike-based sampling module introduces the dilemma of handling data after the final spike emission. An intuitive idea to address this involves incorporating the remaining information into the embedding, aiming to reduce information loss. However, this approach leads to a scenario where neurons, even without firing, accumulate substantial information for the downstream process. This inadvertently aggravates sampling degradation by diminishing the incentive for the sampling module to accurately learn spike timing. Hence, we propose the strategy of Residual Potential Dropout (RPD) to exclude all events following the last spike, enhancing the learning of precise firing moments. To illustrate the efficacy of RPD, we show the potential aggregation distribution with and without RPD. The results, as depicted in Fig. 3, generally reveal a more compact feature distribution with RPD. Moreover, employing

SAT for gradient guidance (shown in the case of ARSNN+SAT), we observe that sampler training devoid of RPD tends to exhibit mode collapse towards the non-firing spectrum with concentrated negative membrane potentials.

4 Experiments

The effectiveness of the proposed approach is initially substantiated in Sec. 4.1. Subsequently, in Sec. 4.2, we compare our comprehensive framework with state-of-the-art event-based methods across benchmark datasets. Additionally, Sec. 4.3 explores the adaptability, hyper-parameter sensitivity, and sampling diversity, while Sec. 4.4 delves into its energy efficiency.

Implementation Details. Our experiments are executed on four RTX 3090 GPUs. We utilize SpikingJelly [12] to enhance the training efficiency of the spike-based backbone. The ADAM optimizer is uniformly applied across all tests, with learning rates of $1e-3$ for Gen1 and $1e-4$ for N-Caltech 101. In alignment with practices from [19, 22], data augmentation techniques including random Zoom-in and horizontal flipping are employed for both datasets. For GEN-1, event sampling is capped at 200ms prior to the timestamp of labeling to manage data processing duration. Unlike the hard reset used in the sampling module, downstream networks implement a soft reset strategy. Rather than employing a learning rate scheduler, we leverage model weight smoothing during training through the use of an exponential moving average with a momentum of 0.9999.

Benchmark Datasets. The Neuromorphic-Caltech 101 (N-Caltech 101) dataset [44], captured by an ATIS event camera [47] traversing 101 object categories via three saccades, comprises 8,246 event streams, each embodying 300 ms of saccades alongside bounding box annotations. We partition this dataset into an 8:2 split for training and validation. The Prophesee Gen1 dataset [10] presents another rigorous neuromorphic benchmark, offering over 39 hours of automotive recordings with more than 228k car and 28k pedestrian annotations for event-based detection in diverse driving scenarios. Adhering to the original evaluation protocol, prediction boxes with either a side length below 20 pixels or a diagonal shorter than 30 pixels are excluded after non-maximum suppression.

4.1 Ablation Study

In this section, we conduct a comparative analysis to ascertain the efficacy of individual components within the proposed sampling module as detailed in Table 1. In addition to comparing with the common event count approach, we introduce two novel embedding strategies leveraging SNNs and RSNNs, predicated on potential aggregation as detailed in Eq. (12). The results show that the integration of recurrent synaptic connections significantly enhances network performance on both datasets, with observed improvements of 6.7% on N-Caltech 101 and 4.9% on Gen1. Notably, employing the SAT and RPD modules in isolation with adaptive sampling sometimes results in a performance decline compared to RSNN (58.6% vs. 63.4% in mAP_{50} on N-Caltech 101). Conversely, when SAT

Table 1: Ablation Study: performance comparison between the conventional histogram method and the proposed spike-based embedding approaches, with and without the adaptive sampling mechanism.

Method	RPD SAT		N-Caltech 101		Gen1	
			mAP ₅₀	mAP _{50:95}	mAP ₅₀	mAP _{50:95}
Event Count	-	-	0.587	0.369	0.611	0.321
SNN	-	-	0.567	0.367	0.670	0.366
RSNN	-	-	0.634	0.412	0.719	0.399
ARSNN	×	×	0.600	0.398	0.687	0.373
ARSNN	✓	×	0.586	0.391	0.714	0.393
ARSNN	×	✓	0.592	0.376	0.714	0.398
ARSNN	✓	✓	0.664	0.437	0.731	0.409

and RPD are synergistically combined within the SNN framework, there is a significant performance improvement, yielding increases of 3.0% and 1.2% in mAP₅₀ over RSNN on the N-Caltech 101 and Gen1 datasets, respectively. This demonstrates the critical importance of integrating these components to achieve optimal network performance.

4.2 Performance Comparison

Next, we evaluate our proposed method against existing techniques on the Gen1 and N-Caltech 101 datasets. In addition to the proposed ARSNN in the embedding module, we adopt PLIF [14] neurons with learnable decay and tdBN [65] across the other spiking layers to improve the overall efficacy of SNNs. The models, sized at 8.92M and 25.3M parameters, mirror the configurations of YOLOX-S and YOLOX-M [17] respectively, achieved through scaling the network width. As evidenced in Table 2, our technique outperforms the state-of-the-art spike-based model [53] in performance metrics (0.354 vs. 0.310 mAP_{50:95}) while operating with a reduced parameter (8.92 M vs. 14.40 M) under three time steps. Even compared with ANNs that feature well-designed attention mechanisms [19] and recurrent architectures [32, 46], our strategy maintains competitiveness and notably marks the first instance of achieving over 40% COCO mAP on Gen1 through sparse spike-driven computations, thereby enhancing energy efficiency as detailed in Sec. 4.4. With regards to N-Caltech 101, to the best of our knowledge, our approach represents the first spike-based solution to attain competitive performance, setting a new benchmark in the field.

In object detection, modules are designed for specific roles: backbones extract features, Feature Pyramid Networks (FPN) fuse multi-scale features, and detection heads handle coordinate regression and object recognition. We examined the effects of sparse spike representation by integrating a non-spiking detection head and FPN into a hybrid architecture. As shown in Table 2, a spiking FPN within a compact 8.92M network outperforms its non-spiking counterpart, indicating that spike-based architectures might offer regularization advantages for event-driven detection. However, spiking detection heads within constrained time steps appear to reduce network performance.

Table 2: Performance comparison with the state-of-the-art methods on Gen1.

Method	Embedding	Backbone	Head	Temporal	#Params	Timestep	mAP ₅₀	mAP _{50:95}
RED [46]	Event Volum	CNN+RNN	SSD	Yes	24.1M	-	-	0.40
RVT [19]	HIST.	Transformer+RNN	YOLOX	Yes	18.5M	21	-	0.475
EGO-12 [69]	EGO-12	Transformer	YOLOv6	No	-	-	-	0.504
AEGNN [49]	Graph	GNN	YOLO	No	20.0M	-	-	0.163
NVS-S [34]	Graph	GNN	YOLO	No	0.9M	-	-	0.086
TAF [38]	CNN	CNN	YOLOX	No	14.8M	-	-	0.454
ASTMNet [32]	1D TCNN	CNN+RNN	SSD	Yes	>100M	3	-	0.467
MatrixLSTM [4]	LSTM	CNN	YOLOv3	Yes	61.5M	-	-	0.310
VC-DenseNet [8]	Voxel Cube	SNN	SSD	Yes	8.2M	5	-	0.189
VC-MobileNet [8]	Voxel Cube	SNN	SSD	Yes	12.64M	5	-	0.174
LT-SNN [25]	HIST.	SNN	YOLOv2	Yes	-	-	-	0.298
KD-SNN [2]	HIST.	SNN	CenterNet	Yes	12.97M	5	-	0.229
EMS-ResNet10 [53]	HIST.	SNN	YOLOv3	Yes	6.2M	5	0.547	0.267
EMS-ResNet18 [53]	HIST.	SNN	YOLOv3	Yes	9.34M	5	0.565	0.286
EMS-ResNet34 [53]	HIST.	SNN	YOLOv3	Yes	14.40M	5	0.590	0.310
TR-YOLO [61]	HIST.	SNN	YOLOv3	Yes	8.7M	3	0.451	-
EAS-SNN	ARSNN	SNN	YOLOX ^o	Yes	25.3M	3	0.731	0.409
			YOLOX [*]	Yes	25.3M	3	0.718	0.393
			YOLOX [!]	Yes	25.3M	3	0.699	0.375
EAS-SNN	ARSNN	SNN	YOLOX ^o	Yes	8.92M	3	0.687	0.372
			YOLOX [*]	Yes	8.92M	3	0.692	0.372
			YOLOX [!]	Yes	8.92M	3	0.675	0.354

[†] denotes the model uses a spiking backbone, a spiking feature pyramid network, and a spiking detection head.

^{*} denotes the model uses a spiking backbone, a spiking feature pyramid network, and a non-spiking detection head.

^o denotes the model uses a spiking backbone, a non-spiking feature pyramid network, and a non-spiking detection head.

Table 3: Performance comparison with the existing methods on N-Caltech 101.

Method	Embedding	Backbone	Head	Temporal	#Params	Timestep	mAP ₅₀	mAP _{50:95}
YOLO [3]	Leaky Surface	CNN	YOLO	No	-	-	0.398	-
AEGNN [49]	Graph	GNN	YOLO	No	20.0M	-	0.595	-
NVS-S [34]	Graph	GNN	YOLO	No	0.9M	-	0.346	-
ASNet [41]	HIST.	CNN	YOLO	No	-	-	0.643	-
ASNet [41]	QUE.	CNN	YOLO	No	-	-	0.615	-
EAS-SNN	ARSNN	SNN	YOLO-X	Yes	25.3M	3	0.664	0.437
EAS-SNN	ARSNN	SNN	YOLO-X	Yes	8.92M	3	0.538	0.338

4.3 Experimental Analysis

Scalability to Dense Neural Network: In this section, our objective is to validate the efficacy of the proposed adaptive sampling technique within conventional dense neural networks. To this end, we configure to transmit only the initial aggregated potential to the subsequent networks. Fig. 4b displays the mAP₅₀ training curves on the N-Caltech 101 dataset, comparing different methods. The combination of ARSNN with SAT and RPD demonstrates promising performance improvements, while ARSNN with SAT or RPD alone leads to declined performance, highlighting the synergistic benefits of our proposed modules. Additionally, introducing recurrent synaptic connections further enhances spike-based embedding performance. These results validate the adaptability of our sampling module for integration into dense neural networks.

Impact of Early Aggregation: We investigate the influence of early aggregation, as defined in Eq. (4), by modulating the aggregation step T_m on Gen1 using spiking YOLOX-S. Here, the first three slices sampling from T_m -step inputs are

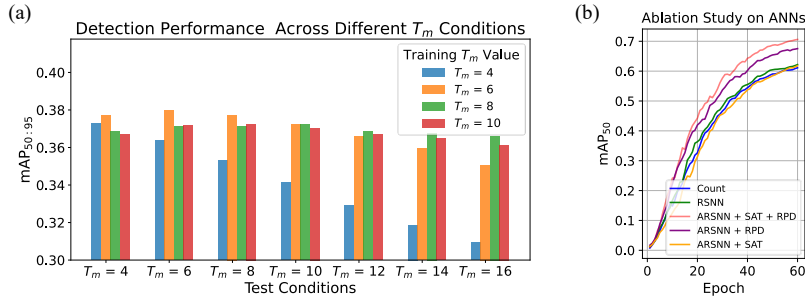


Fig. 4: (a) Assessing the scalability of the early aggregation step T_m in mismatched testing scenarios on Gen1. (b) Evaluating the effectiveness of the proposed adaptive sampling mechanism within conventional dense neural networks on N-Caltech 101.

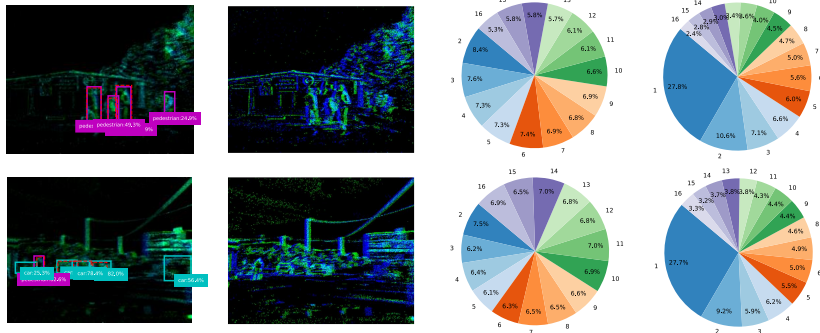


Fig. 5: Exploring the behavior of sampling module. The first column illustrates bounding boxes of prediction, whereas the second column provides pixel-wise firing count of spike neurons. The third and fourth columns, respectively, depict the distribution of neuron firing time and the sampling duration, quantified as the inter-spike interval.

aggregated and fed sequentially into a spike-based backbone. The parameter T_m indicates the temporal resolution of inputs, where a higher T_m corresponds to a finer granularity. As depicted in Fig. 4a, optimal performance is generally observed when T_m remains consistent between the training and testing phases. Notably, the model trained with $T_m = 4$, sustains over 30% $mAP_{50:95}$, despite a fourfold reduction in granularity. Overall, models trained with $T_m = 8$ demonstrate considerable robustness, delivering promising performance under all tested conditions.

Distribution of Event Sampling: In this part, we employ the model trained under $T_m = 8$ and examine the behavior of each neuron while using $T_m = 16$ for inference. The sampling intervals of various spiking neurons are shown in the last column of Fig. 5, which demonstrates significant variability. The longest sample covers the full input, while the shortest sample only includes the input of one time step. Here, we disregard the neurons without spike firing, which typically make up 80%+ due to the sparse event input. Additionally, compared to the

Table 4: Comparison of energy consumption based on number of synaptic operations.

Module	YOLOX-M		Spiking YOLOX-M			YOLOX-S		Spiking YOLOX-S		
	MAC(G)	Energy(mJ)	AC(G)	MAC(G)	Energy(mJ)	MAC(G)	Energy(mJ)	AC(G)	MAC(G)	Energy(mJ)
Embedding	0	0	0.02	1.63	7.52	0	0	0.02	1.63	7.52
Backbone	16.21	74.57	8.49	1.41	14.12	5.24	24.10	2.66	0.71	5.64
FPN	8.19	37.68	3.40	0	3.06	2.63	12.09	1.26	0	1.14
Head	11.33	52.10	3.78	0	3.40	5.04	23.17	1.79	0	1.61
Total	35.73	164.35(1×)	15.68	3.04	28.10(5.85×)	12.90	59.35(1×)	5.74	2.34	15.91(3.73×)

event count representation in the first column, the image of the firing count in the second column offers a clearer estimation of the scene.

4.4 Energy Efficiency

While ANNs execute a fixed number of multiplication-and-accumulation (MAC) operations determined by their architecture, SNNs on neuromorphic hardware utilize input-conditioned spikes for sparse accumulation (AC) operations, enhancing energy efficiency. To assess the energy efficiency of SNNs, we compute the average AC operation count across Gen1, as detailed in Table 4. The energy cost for 32-bit floating-point addition (AC) and multiply-and-add (MAC) are quantified at 0.9 pJ and 4.6 pJ per operation, respectively, following [23]. The results show a significant reduction in energy consumption (5.85× for YOLOX-M and 3.73× for YOLOX-S) with spike-driven computation. It is worth noting that, for ANNs, we omit the energy consumption of the embedding phase, offering a comparatively conservative estimate of power savings. The detailed firing rates and more results across different models can be found in Supplementary Materials.

5 Conclusion

We introduce the Adaptive Sampling technique with Recurrent Spiking Neural Networks (ARSNN), enhanced by Residual Potential Dropout (RPD) and Spike-Aware Training (SAT) specifically to mitigate performance degradation in event-based sampling. Integrated with a spike-based architecture in the downstream neural network, our comprehensive framework, EAS-SNN, achieves superior performance relative to existing spike-based detection methods, delivering enhanced energy efficiency in comparison to ANNs. To the best of our knowledge, it is the first effort toward end-to-end optimization for event-based sampling and representation. Additionally, we demonstrate the versatility of our proposed sampling technique through its application to dense neural networks. Despite our exploration of the robustness across varying granularity of early aggregation, the ultimate goal is the development of a spike-based sampler that can precisely synchronize with the temporal granularity of raw event streams, measured in microseconds, without necessitating early aggregation. Our future work will focus on achieving this granularity, pending advancements in neuromorphic computing infrastructure.

References

1. Akopyan, F., Sawada, J., Cassidy, A., Alvarez-Icaza, R., Arthur, J., Merolla, P., Imam, N., Nakamura, Y., Datta, P., Nam, G.J., et al.: Truenorth: Design and tool flow of a 65 mw 1 million neuron programmable neurosynaptic chip. *IEEE transactions on computer-aided design of integrated circuits and systems* **34**(10), 1537–1557 (2015) [2](#)
2. Bodden, L., Schwaiger, F., Ha, D.B., Kreuzberg, L., Behnke, S.: Spiking centernet: A distillation-boosted spiking neural network for object detection. *arXiv preprint arXiv:2402.01287* (2024) [12](#)
3. Cannici, M., Ciccone, M., Romanoni, A., Matteucci, M.: Asynchronous convolutional networks for object detection in neuromorphic cameras. In: *Proceedings of the IEEE/CVF Conference on Computer Vision and Pattern Recognition Workshops*. pp. 0–0 (2019) [2](#), [4](#), [12](#)
4. Cannici, M., Ciccone, M., Romanoni, A., Matteucci, M.: A differentiable recurrent surface for asynchronous event-based data. In: *The European Conference on Computer Vision (ECCV)* (August 2020) [4](#), [12](#)
5. Cao, J., Sun, M., Wang, Z., Cheng, H., Zhang, Q., Xu, R.: BEEF: Building a bridge from event to frame (2024), <https://openreview.net/forum?id=IHedM0Zem9> [2](#), [4](#)
6. Chen, X., Wu, J., Tang, H., Ren, Q., Tan, K.C.: Unleashing the potential of spiking neural networks for sequential modeling with contextual embedding. *arXiv preprint arXiv:2308.15150* (2023) [4](#)
7. Chowdhury, S.S., Rathi, N., Roy, K.: Towards ultra low latency spiking neural networks for vision and sequential tasks using temporal pruning. In: *European Conference on Computer Vision*. pp. 709–726. Springer (2022) [4](#)
8. Cordone, L., Miramond, B., Thierion, P.: Object detection with spiking neural networks on automotive event data. In: *2022 International Joint Conference on Neural Networks (IJCNN)*. pp. 1–8. IEEE (2022) [2](#), [4](#), [12](#)
9. Davies, M., Srinivasa, N., Lin, T.H., Chinya, G., Cao, Y., Choday, S.H., Dimou, G., Joshi, P., Imam, N., Jain, S., et al.: Loihi: A neuromorphic manycore processor with on-chip learning. *Ieee Micro* **38**(1), 82–99 (2018) [2](#)
10. De Tournemire, P., Nitti, D., Perot, E., Migliore, D., Sironi, A.: A large scale event-based detection dataset for automotive. *arXiv preprint arXiv:2001.08499* (2020) [10](#)
11. Duan, C., Ding, J., Chen, S., Yu, Z., Huang, T.: Temporal effective batch normalization in spiking neural networks. *Advances in Neural Information Processing Systems* **35**, 34377–34390 (2022) [4](#)
12. Fang, W., Chen, Y., Ding, J., Yu, Z., Masquelier, T., Chen, D., Huang, L., Zhou, H., Li, G., Tian, Y.: Spikingjelly: An open-source machine learning infrastructure platform for spike-based intelligence. *Science Advances* **9**(40), eadi1480 (2023) [10](#)
13. Fang, W., Yu, Z., Chen, Y., Huang, T., Masquelier, T., Tian, Y.: Deep residual learning in spiking neural networks. *Advances in Neural Information Processing Systems* **34**, 21056–21069 (2021) [4](#)
14. Fang, W., Yu, Z., Chen, Y., Masquelier, T., Huang, T., Tian, Y.: Incorporating learnable membrane time constant to enhance learning of spiking neural networks. In: *ICCV*. pp. 2661–2671 (2021) [2](#), [4](#), [8](#), [11](#)
15. Finateu, T., Niwa, A., Matolin, D., Tsuchimoto, K., Mascheroni, A., Reynaud, E., Mostafalu, P., Brady, F., Chotard, L., LeGoff, F., et al.: 5.10 a 1280× 720 back-illuminated stacked temporal contrast event-based vision sensor with 4.86 μm pixels, 1.066 geps readout, programmable event-rate controller and compressive data-formatting pipeline. In: *2020 IEEE International Solid-State Circuits Conference-(ISSCC)*. pp. 112–114. IEEE (2020) [2](#)

16. Gallego, G., Delbrück, T., Orchard, G., Bartolozzi, C., Taba, B., Censi, A., Leutenegger, S., Davison, A.J., Conradt, J., Daniilidis, K., et al.: Event-based vision: A survey. *IEEE transactions on pattern analysis and machine intelligence* **44**(1), 154–180 (2020) [2](#)
17. Ge, Z., Liu, S., Wang, F., Li, Z., Sun, J.: Yolox: Exceeding yolo series in 2021. arXiv preprint arXiv:2107.08430 (2021) [11](#)
18. Gehrig, D., Loquercio, A., Derpanis, K.G., Scaramuzza, D.: End-to-end learning of representations for asynchronous event-based data. In: *Proceedings of the IEEE/CVF International Conference on Computer Vision*. pp. 5633–5643 (2019) [2](#)
19. Gehrig, M., Scaramuzza, D.: Recurrent vision transformers for object detection with event cameras. In: *Proceedings of the IEEE/CVF Conference on Computer Vision and Pattern Recognition*. pp. 13884–13893 (2023) [2](#), [4](#), [5](#), [10](#), [11](#), [12](#)
20. Guo, Y., Chen, Y., Zhang, L., Liu, X., Wang, Y., Huang, X., Ma, Z.: Im-loss: information maximization loss for spiking neural networks. *Advances in Neural Information Processing Systems* **35**, 156–166 (2022) [4](#)
21. Guo, Y., Chen, Y., Zhang, L., Wang, Y., Liu, X., Tong, X., Ou, Y., Huang, X., Ma, Z.: Reducing information loss for spiking neural networks. In: *European Conference on Computer Vision (Cham: Springer)*. p. 36–52 (2022) [4](#)
22. Hamaguchi, R., Furukawa, Y., Onishi, M., Sakurada, K.: Hierarchical neural memory network for low latency event processing. In: *Proceedings of the IEEE/CVF Conference on Computer Vision and Pattern Recognition*. pp. 22867–22876 (2023) [2](#), [4](#), [10](#)
23. Han, S., Pool, J., Tran, J., Dally, W.: Learning both weights and connections for efficient neural network. *Advances in Neural Information Processing Systems* **28** (2015) [14](#)
24. Hao, Z., Shi, X., Huang, Z., Bu, T., Yu, Z., Huang, T.: A progressive training framework for spiking neural networks with learnable multi-hierarchical model. In: *The Twelfth International Conference on Learning Representations (2024)*, <https://openreview.net/forum?id=g52tgL8jy6> [4](#)
25. Hassan, A., Meng, J., sun Seo, J.: LT-SNN: Self-adaptive spiking neural network for event-based classification and object detection (2023), <https://openreview.net/forum?id=oyzMyylgINj> [12](#)
26. Kim, Y., Li, Y., Park, H., Venkatesha, Y., Hambitzer, A., Panda, P.: Exploring temporal information dynamics in spiking neural networks. In: *Proceedings of the AAAI Conference on Artificial Intelligence*. vol. 37, pp. 8308–8316 (2023) [7](#)
27. Kim, Y., Li, Y., Park, H., Venkatesha, Y., Panda, P.: Neural architecture search for spiking neural networks. In: *European Conference on Computer Vision*. pp. 36–56. Springer (2022) [4](#)
28. Kugele, A., Pfeil, T., Pfeiffer, M., Chicca, E.: Hybrid snn-ann: Energy-efficient classification and object detection for event-based vision. In: *DAGM German Conference on Pattern Recognition*. pp. 297–312. Springer (2021) [2](#)
29. Kugele, A., Pfeil, T., Pfeiffer, M., Chicca, E.: How many events make an object? improving single-frame object detection on the 1 mpx dataset. In: *Proceedings of the IEEE/CVF Conference on Computer Vision and Pattern Recognition*. pp. 3912–3921 (2023) [4](#)
30. Lagorce, X., Meyer, C., Ieng, S.H., Filliat, D., Benosman, R.: Asynchronous event-based multikernel algorithm for high-speed visual features tracking. *IEEE transactions on neural networks and learning systems* **26**(8), 1710–1720 (2014) [2](#), [4](#)

31. Lagorce, X., Orchard, G., Galluppi, F., Shi, B.E., Benosman, R.B.: Hots: a hierarchy of event-based time-surfaces for pattern recognition. *IEEE transactions on pattern analysis and machine intelligence* **39**(7), 1346–1359 (2016) [2](#)
32. Li, J., Li, J., Zhu, L., Xiang, X., Huang, T., Tian, Y.: Asynchronous spatio-temporal memory network for continuous event-based object detection. *IEEE Transactions on Image Processing* **31**, 2975–2987 (2022) [2](#), [4](#), [5](#), [11](#), [12](#)
33. Li, J., Wang, X., Zhu, L., Li, J., Huang, T., Tian, Y.: Retinomorph object detection in asynchronous visual streams. In: *Proceedings of the AAAI Conference on Artificial Intelligence*. vol. 36, pp. 1332–1340 (2022) [4](#)
34. Li, Y., Zhou, H., Yang, B., Zhang, Y., Cui, Z., Bao, H., Zhang, G.: Graph-based asynchronous event processing for rapid object recognition. In: *Proceedings of the IEEE/CVF International Conference on Computer Vision*. pp. 934–943 (2021) [2](#), [4](#), [12](#)
35. Li, Y., Guo, Y., Zhang, S., Deng, S., Hai, Y., Gu, S.: Differentiable spike: Rethinking gradient-descent for training spiking neural networks. *NeurIPS* **34** (2021) [2](#), [4](#)
36. Lian, S., Shen, J., Liu, Q., Wang, Z., Yan, R., Tang, H.: Learnable surrogate gradient for direct training spiking neural networks. In: *Proceedings of the Thirty-Second International Joint Conference on Artificial Intelligence, IJCAI-23*. pp. 3002–3010 (2023) [4](#)
37. Lichtsteiner, P., Posch, C., Delbruck, T.: A 128×128 120 db 15 μ s latency asynchronous temporal contrast vision sensor. *IEEE Journal of Solid-State Circuits* **43**(2), 566–576 (2008). <https://doi.org/10.1109/JSSC.2007.914337> [2](#)
38. Liu, B., Xu, C., Yang, W., Yu, H., Yu, L.: Motion robust high-speed light-weighted object detection with event camera. *IEEE Transactions on Instrumentation and Measurement* (2023) [2](#), [4](#), [12](#)
39. Liu, Q., Xing, D., Tang, H., Ma, D., Pan, G.: Event-based action recognition using motion information and spiking neural networks. In: *IJCAI*. pp. 1743–1749 (2021) [2](#)
40. Messikommer, N., Gehrig, D., Gehrig, M., Scaramuzza, D.: Bridging the gap between events and frames through unsupervised domain adaptation. *IEEE Robotics and Automation Letters* **7**(2), 3515–3522 (2022) [4](#)
41. Messikommer, N., Gehrig, D., Loquercio, A., Scaramuzza, D.: Event-based asynchronous sparse convolutional networks. In: *Computer Vision–ECCV 2020: 16th European Conference, Glasgow, UK, August 23–28, 2020, Proceedings, Part VIII* 16. pp. 415–431. Springer (2020) [2](#), [12](#)
42. Mirsadeghi, M., Shalchian, M., Kheradpisheh, S.R., Masquelier, T.: Stidi-bp: Spike time displacement based error backpropagation in multilayer spiking neural networks. *Neurocomputing* **427**, 131–140 (2021) [4](#)
43. Mostafa, H.: Supervised learning based on temporal coding in spiking neural networks. *IEEE transactions on neural networks and learning systems* **29**(7), 3227–3235 (2017) [4](#)
44. Orchard, G., Jayawant, A., Cohen, G.K., Thakor, N.: Converting static image datasets to spiking neuromorphic datasets using saccades. *Frontiers in neuroscience* **9**, 437 (2015) [10](#)
45. Pei, J., Deng, L., Song, S., Zhao, M., Zhang, Y., Wu, S., Wang, G., Zou, Z., Wu, Z., He, W., et al.: Towards artificial general intelligence with hybrid tianjic chip architecture. *Nature* **572**(7767), 106–111 (2019) [2](#)
46. Perot, E., De Tournemire, P., Nitti, D., Masci, J., Sironi, A.: Learning to detect objects with a 1 megapixel event camera. *Advances in Neural Information Processing Systems* **33**, 16639–16652 (2020) [2](#), [4](#), [5](#), [11](#), [12](#)

47. Posch, C., Matolin, D., Wohlgenannt, R.: A qvga 143 db dynamic range frame-free pwm image sensor with lossless pixel-level video compression and time-domain cds. *IEEE Journal of Solid-State Circuits* **46**(1), 259–275 (2010) [10](#)
48. Ren, D., Ma, Z., Chen, Y., Peng, W., Liu, X., Zhang, Y., Guo, Y.: Spiking point-net: Spiking neural networks for point clouds. *Advances in Neural Information Processing Systems* **36** (2024) [4](#)
49. Schaefer, S., Gehrig, D., Scaramuzza, D.: Aegnn: Asynchronous event-based graph neural networks. In: *Proceedings of the IEEE/CVF conference on computer vision and pattern recognition*. pp. 12371–12381 (2022) [2](#), [4](#), [12](#)
50. Serrano-Gotarredona, T., Linares-Barranco, B.: A 128×128 1.5% contrast sensitivity 0.9% fpn $3 \mu\text{s}$ latency 4 mw asynchronous frame-free dynamic vision sensor using transimpedance preamplifiers. *IEEE Journal of Solid-State Circuits* **48**(3), 827–838 (2013) [2](#)
51. Shrestha, S.B., Orchard, G.: Slayer: Spike layer error reassignment in time. *arXiv preprint arXiv:1810.08646* (2018) [2](#), [4](#), [8](#)
52. Sironi, A., Brambilla, M., Bourdis, N., Lagorce, X., Benosman, R.: Hats: Histograms of averaged time surfaces for robust event-based object classification. In: *Proceedings of the IEEE conference on computer vision and pattern recognition*. pp. 1731–1740 (2018) [2](#)
53. Su, Q., Chou, Y., Hu, Y., Li, J., Mei, S., Zhang, Z., Li, G.: Deep directly-trained spiking neural networks for object detection. In: *Proceedings of the IEEE/CVF International Conference on Computer Vision*. pp. 6555–6565 (2023) [2](#), [4](#), [5](#), [11](#), [12](#)
54. Wang, D., Jia, X., Zhang, Y., Zhang, X., Wang, Y., Zhang, Z., Wang, D., Lu, H.: Dual memory aggregation network for event-based object detection with learnable representation. *arXiv preprint arXiv:2303.09919* (2023) [4](#)
55. Wang, Z., Jiang, R., Lian, S.J., Yan, R., Tang, H.: Adaptive smoothing gradient learning for spiking neural networks. In: *International Conference on Machine Learning* (2023) [2](#), [4](#)
56. Werbos, P.J.: Generalization of backpropagation with application to a recurrent gas market model. *Neural networks* **1**(4), 339–356 (1988) [8](#)
57. Wu, J., Yılmaz, E., Zhang, M., Li, H., Tan, K.C.: Deep spiking neural networks for large vocabulary automatic speech recognition. *Frontiers in neuroscience* **14**, 199 (2020) [4](#)
58. Wu, Y., Deng, L., Li, G., Zhu, J., Shi, L.: Spatio-temporal backpropagation for training high-performance spiking neural networks. *Frontiers in neuroscience* **12**, 331 (2018) [2](#), [4](#), [8](#)
59. Yao, M., Gao, H., Zhao, G., Wang, D., Lin, Y., Yang, Z., Li, G.: Temporal-wise attention spiking neural networks for event streams classification. In: *ICCV*. pp. 10221–10230 (2021) [4](#)
60. Yao, X., Li, F., Mo, Z., Cheng, J.: Glif: A unified gated leaky integrate-and-fire neuron for spiking neural networks. *arXiv preprint arXiv:2210.13768* (2022) [4](#)
61. Yuan, M., Zhang, C., Wang, Z., Liu, H., Pan, G., Tang, H.: Trainable spiking-yolo for low-latency and high-performance object detection. *Neural Networks* **172**, 106092 (2024) [4](#), [5](#), [12](#)
62. Zenke, F., Vogels, T.P.: The remarkable robustness of surrogate gradient learning for instilling complex function in spiking neural networks. *Neural Computation* **33**(4), 899–925 (2021) [2](#), [4](#)
63. Zhang, M., Wang, J., Wu, J., Belatreche, A., Amornpaisannon, B., Zhang, Z., Miriyala, V.P.K., Qu, H., Chua, Y., Carlson, T.E., et al.: Rectified linear postsynap-

- tic potential function for backpropagation in deep spiking neural networks. *IEEE transactions on neural networks and learning systems* **33**(5), 1947–1958 (2021) [4](#)
64. Zhang, W., Li, P.: Temporal spike sequence learning via backpropagation for deep spiking neural networks. *Advances in Neural Information Processing Systems* **33**, 12022–12033 (2020) [4](#)
 65. Zheng, H., Wu, Y., Deng, L., Hu, Y., Li, G.: Going deeper with directly-trained larger spiking neural networks. In: *AAAI 2021*. pp. 11062–11070. AAAI Press (2021) [4](#), [11](#)
 66. Zhou, Z., Zhu, Y., He, C., Wang, Y., Yan, S., Tian, Y., Yuan, L.: Spikformer: When spiking neural network meets transformer. *arXiv preprint arXiv:2209.15425* (2022) [4](#)
 67. Zhu, Y., Fang, W., Xie, X., Huang, T., Yu, Z.: Exploring loss functions for time-based training strategy in spiking neural networks. *Advances in Neural Information Processing Systems* **36** (2024) [4](#)
 68. Zhu, Y., Yu, Z., Fang, W., Xie, X., Huang, T., Masquelier, T.: Training spiking neural networks with event-driven backpropagation. *Advances in Neural Information Processing Systems* **35**, 30528–30541 (2022) [2](#)
 69. Zubić, N., Gehrig, D., Gehrig, M., Scaramuzza, D.: From chaos comes order: Ordering event representations for object recognition and detection. In: *Proceedings of the IEEE/CVF International Conference on Computer Vision*. pp. 12846–12856 (2023) [2](#), [4](#), [12](#)